Hydroxamate-Based Selective Macrophage Elastase (MMP-12) Inhibitors and Radiotracers for Molecular Imaging

Kiran Gona, Jakub Toczek, Yunpeng Ye, Nowshin Sanzida, Arvene Golbazi, Parnaz Boodagh, Mani Salarian, Jae-Joon Jung, Saranya Rajendran, Gunjan Kukreja, et al.

HHS Public Access

Author manuscript

J Med Chem. Author manuscript; available in PMC 2021 June 10.

Published in final edited form as:

J Med Chem. 2020 December 10; 63(23): 15037–15049. doi:10.1021/acs.jmedchem.0c01514.

Hydroxamate based Selective Macrophage Elastase (MMP-12) Inhibitors and Radiotracers for Molecular Imaging

Kiran Gona[#,‖], **Jakub Toczek**[#,‖], **Yunpeng Ye**[#,‖], **Nowshin Sanzida**[#,‖], **Arvene Golbazi**[#,‖], **Parnaz Boodagh**[#,‖], **Mani Salarian**[#,‖], **Jae-Joon Jung**[#,‖], **Saranya Rajendran**[#,‖], **Gunjan Kukreja**[#,‖], **Terence L. Wu**[§], **Laurent Devel**[‡], **Mehran M. Sadeghi**[#,‖,*]

[#]Cardiovascular Molecular Imaging Laboratory, Section of Cardiovascular Medicine and Yale Cardiovascular Research Center, Yale University School of Medicine, New Haven, CT-06511 (USA);

[‖]Veterans Affairs Connecticut Healthcare System, West Haven, CT-06516 (USA);

[§]Yale West Campus Analytical Core, Yale University, West Haven, CT-06516 (USA);

[‡]CEA, INRAE, Medicaments et Technologies pour la Sante (MTS), SIMoS, Université Paris-Saclay, 91191, Gif-sur-Yvette, (France)

Abstract

Macrophage elastase [matrix metalloproteinase (MMP)-12] is the most upregulated MMP in abdominal aortic aneurysm (AAA) and hence MMP-12-targeted imaging may predict AAA progression and rupture risk. Here, we report the design, synthesis and evaluation of three novel hydroxamate-based selective MMP-12 inhibitors (CGA, CGA-1 & AGA) and the methodology to obtain MMP-12 selectivity from hydroxamate-based panMMP inhibitors. Also, we report two ^{99m}Tc-radiotracers [^{99m}Tc]-AGA-1 and [^{99m}Tc]-AGA-2, derived from AGA. [^{99m}Tc]-AGA-2 displayed faster blood clearance in mice and better radiochemical stability compared to [^{99m}Tc]-AGA-1. Based on this, [^{99m}Tc]-AGA-2 was chosen as the lead tracer and tested in murine AAA. [^{99m}Tc]-AGA-2 uptake detected by autoradiography was significantly higher in AAA compared to normal aortic regions. Specific binding of the tracer to MMP-12 was demonstrated through ex vivo competition. Accordingly, this study introduces a novel family of MMP-12-selective inhibitors and tracers, paving the way for further development of these agents as therapeutic and imaging agents.

Graphical Abstract

[*]Corresponding author: Mehran M. Sadeghi. Professor of Medicine (Cardiology), Yale School of Medicine. Phone: 203 737 6954; Fax: 203 937 3884; mehran.sadeghi@yale.edu.

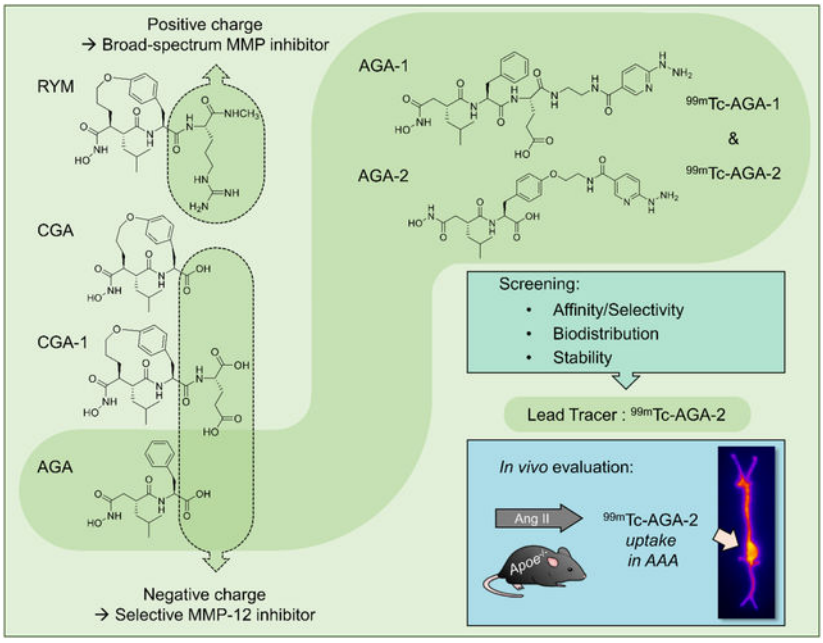

INTRODUCTION

Matrix metalloproteinases (MMPs) are calcium–dependent zinc endopeptidases that belong to the family of metzincins. These enzymes are capable of degrading different components of extracellular matrix (ECM),[1] the regulated breakdown of which is essential for many biological processes, including tissue remodeling and resorption.[2–4] Dysregulated ECM degradation contributes to a wide range of diseases such as cancer, arthritis, nephritis, heart failure, atherosclerosis and aneurysm.[5–12] MMPs also participates in pathophysiological processes by regulating the release or activation of chemokines, cytokines, growth factors, and other bioactive molecules.[13–15] Typically, MMPs are secreted as inactive zymogens and require proteolytic activation by tissue or plasma proteinases to become active. MMP activity is also regulated by endogenous regulators called tissue inhibitors of metalloproteinases. Owing to their important role, MMPs are considered as promising targets for the development of new therapeutic and diagnostic tools. Based on this, several broad spectrum MMP inhibitors (MMPIs) have been developed as therapeutic agents.[6, 16–19] In addition, single photon emission computed tomography (SPECT) and positron emission tomography (PET) tracers are under development and evaluation in preclinical animal models for molecular imaging of cardiovascular, as well as other diseases.[20–22] Several MMPIs have failed as therapeutic agents in late-phase clinical trials, mainly due to musculoskeletal side effects, possibly related to their lack of selectivity and the complexity of their actions.[19] These draw backs can be potentially overcome by developing more selective MMP inhibitors.

MMP-12 or macrophage elastase, a 55kDa protein best known for its elastase activity, is produced by macrophages and a number of other cell type.[23] MMP-12 is implicated in the pathogenesis of abdominal aortic aneurysm (AAA). While normal arteries express low levels of MMP-12, it is highly upregulated in aneurysmal arteries in humans and animal models of

AAA.[24–26] Accordingly, selective MMP-12 targeting may be a potential therapeutic, as well as molecular imaging target in these setting.[23, 25, 27, 28]

Several hydroxamate-based succinic acid derivatives with α, P1', P2' and P3' substituents have been developed as panMMP inhibitors, where the hydroxamate group acts as a Zinc Binding Group (ZBG).[22, 29–33] The structure-activity-relationship experiments performed on these series but also those on other series of MMPIs have elucidated the structural requirements to achieve potency and selectivity. In this respect, the hydroxamate function as a strong ZBG mainly drives MMPI potency while the side chain at the P1′-segment, which interacts within the hydrophobic S1′ pocket, allows to modulate their selectivity, with significant differences when the length and flexibility of this side chain is modified. The impact of P1' on MMPI selectivity is even more pronounced when weaker ZGBs than hydroxamate moiety are used.[34] Similarly, substituents at α, P2' and P3' positions have often minimal effects in hydroxamate series but have more impact when other ZBGs are employed. Accordingly, two glutamate residues in P2' and P3' position within a pseudo peptide scaffold containing a phosphinic function as a weak ZBG, and clearly drive the inhibitor selectivity for MMP-12.[35, 36] However, our recent studies on the complex role of the ZBG[36] clearly showed that subtle modulations between the latter and the different substituents along the pseudo peptide backbone have to be carefully considered to achieve selectivity, not excluding the possibility to identify selective binders in the hydroxamate series.

Given the role of MMP-12 in AAA and other pathological processes, we have sought to develop selective MMP-12 inhibitors and their corresponding radiotracers with a considerable selectivity over other metalloproteinases. Anti-succinate based acyclic or cyclic hydroxamate analogues have been extensively studied in the literature as panMMP inhibitors and their chemistry is well established. While keeping the hydrophobic P1′ fragment unchanged on the anti-succinate hydroxamate core, cyclizing the α and P2' positions, and modifying the P3′-segment with a free acid side chain (CGA & CGA-1, Figure 1), we observed selective binding towards MMP-12 when compared with several other MMPs. Keeping in mind the challenges involved in preparing these multi step, multi chiral cyclic analogues, a similar methodology (keeping a free acid side chain) was used to prepare an easily accessible succinyl hydroxamate-based acyclic analogue (AGA, Figure 1), which also displayed selective MMP-12 inhibition. Two precursors for ^{99m}Tc conjugation (AGA-1 & AGA-2, Figure 1) developed based on AGA retained MMP-12 selectivity. The corresponding single photon computed tomography (SPECT) tracers (^{99m}Tc-AGA-1 & ^{99m}Tc-AGA-2, Figure 1) were synthesized and their radiochemical stability, *ex vivo* binding, pharmacokinetics and biodistribution were evaluated and compared. Finally, the tracer displaying the best performance, ^{99m}Tc-AGA-2, was tested in a murine model of AAA in which MMP-12 is upregulated.

RESULTS

Synthesis of selective MMP-12 inhibitors

The synthetic strategy used for the preparation of CGA and CGA-1 is shown in Scheme 1. The anti-succinic acid derivative, (2R,3S)-3-(tert-butoxycarbonyl)-2-isobutylhex-5-enoic

acid, was used as the starting material and converted into its benzyl ester (**1**) using 1,8-diazabicyclo[5.4.0]undec-7-ene (DBU) and benzyl bromide in toluene. The intermediate **2** was prepared by hydroboration of **1** using 9-borabicyclo [3.3.1] nonane (9-BBN) & H_2O_2 in tetrahydrofuran (THF). The hydroxyl intermediate (2) was converted into its bromide derivative using CBr_4 and triphenylphosphine (Ph_3P) in dichloromethane (DCM) to obtain **3**. The benzyl ester group on **3** was deprotected using 10% palladium on carbon (Pd/C) and hydrogen gas in methanol to obtain **4**. L-tyrosine benzyl ester was coupled to the acid, **4**, using 1-Ethyl-3-(3-dimethylaminopropyl) carbodiimide hydrochloride (EDCI) and 1-Hydroxybenzotriazole hydrate (HOBT) in N.N-Dimethyl formamide (DMF) to obtain **5**. The bromo group from alpha-position and the hydroxyl group from P_2' were cyclized using Cs_2CO_3 in anhydrous acetonitrile to give the cyclized intermediate **6**. The t-butyl group on **6** was deprotected using trifluoroacetic acid (TFA) in DCM to obtain **7**, which was coupled with O-benzyl hydroxylamine hydrochloride using HBTU in DMF to obtain **8**. Both benzyl groups on **8** were deprotected using 10% Pd/C and hydrogen gas in methanol to obtain the acid CGA (**9**). Coupling of L-glutamic acid di-*tert*-butyl ester with **9** using EDCI & HOBT in DMF followed by hydrolysis of acid esters resulted in CGA-1 (**11**).

The synthetic strategy used for the preparation of AGA & AGA-1 is shown in Scheme 2. The synthesis started from 4-methylpentanoic acid which was converted to 4-methylpentanoyl chloride using oxalyl chloride in THF at 0 °C. The acid chloride obtained was then converted to intermediate **12** by reacting with (S)-(−)-4-benzyl-2-oxazolidinone in THF at −78 °C. Reacting intermediate **12** with 2.0M Sodium bis(trimethylsilyl)amide solution (NaHMDS) at −78 °C followed by tert-butyl bromoacetate in THF resulted in **13**. The hydrolysis of **13** using a 30% hydrogen peroxide solution and $LiOH\text{-}H_2O$ in THF/H_2O at 0 °C resulted in **14**. L-phenylalanine -*O*Bz ester was coupled with intermediate **14** using EDCI & HOBT in DMF to obtain **15**. The t-butyl group of intermediate **15** was hydrolyzed using TFA in DCM to result in **16**. The acid obtained was coupled with *O*-benzyl hydroxylamine hydrochloride using EDCI & HOBT in DMF to result in intermediate **17**. Both benzyl groups on **17** were deprotected using 10% Pd/C and hydrogen gas in methanol to obtain AGA (**18**).

The Fmoc-L-glutamate benzylester was coupled with N-Boc-ethylenediamine using EDCI & HOBT in DMF to obtain **19**. De-protection of Boc- protecting group using TFA & DCM resulted in **20**, which was coupled with 6-Boc-hydrazinonicotinic acid (boc-HYNIC acid) to result **21**. The Fmoc-group was deprotected using piperidine in DCM to obtain intermediate **22**, which was coupled with intermediate **18** using EDCI & HOBT in DMF to obtain **23**. The benzyl ester was hydrolyzed using 10% Pd/C and hydrogen gas in methanol and de-protection of N-boc using TFA in DCM resulted in AGA-1 (**24**).

The synthetic strategy used for the preparation of AGA-2 is shown in Scheme 3. D-tyrosine alanine *O*-benzyl ester was coupled with the intermediate **14** using EDCI & HOBT in DMF to obtain **25**. The t-butyl group of **25** was hydrolyzed using TFA in DCM led to **26**. The resulting acid was coupled with *O*-benzyl hydroxylamine hydrochloride using EDCI & HOBT in DMF to access **27**. N-boc-protected ethanolamine was coupled with **27** using Cs_2CO_3 in DMF to obtain **28**. The N-boc group was de-protected using TFA in DCM to

obtain **29**, which was coupled with N-boc protected HYNIC acid using HATU & HOAT in DMF to obtain **30**. The N-boc group was de-protected using TFA in DCM to obtain **31**, which following de-protection of di-benzyl groups using 10% Pd/C under hydrogen gas resulted in AGA-2 (**32**).

MMP affinity determination

The inhibition constants (K_i) of CGA, CGA-1 and AGA, as well as the radiolabeling precursors, AGA-1 and AGA-2 were evaluated in comparison with the panMMP inhibitor, RYM for a set of recombinant human (rh)MMPs using an assay involving the cleavage of a fluorogenic substrate, Mca-Lys-Pro-Leu-Gly-Leu-Dpa-Ala-Arg-NH_2. All newly developed inhibitors showed great affinity and selectivity towards rhMMP-12 when compared to a select group of rhMMPs. Accordingly, the cyclic inhibitors, CGA & CGA-1 displayed K_i values of < 2 nM, and acyclic inhibitors, AGA, AGA-1 & AGA-2 displayed K_i values ranging from 7.5 to 12 towards rhMMP-12 (Table 1). The selectivity of cyclic inhibitors for rhMMP-12 relative to other MMPs tested ranged from at least 12 folds (for CGA-1 against rhMMP-7) to 28 folds (for CGA against rhMMP-13). Amongst acyclic inhibitors, AGA-2 displayed the highest selectivity (17 folds against rhMMP-9). Finally, like their binding to rhMMP-12, all inhibitors showed high affinity for murine MMP-12 (Table S1).

Radiolabeling

^{99m}Tc-labeling of precursors AGA1 and AGA2 was performed according to an established methodology.[37, 38] Both ^{99m}Tc-AGA-1 and ^{99m}Tc-AGA-2 showed more than 95 % conversion of $^{99m}TcO_4^-$ to its radiolabeling product with retention times of 18.0 min & 22.6 min, respectively. Both ^{99m}Tc-AGA-1 and ^{99m}Tc-AGA-2 were consistently obtained with >95% radiochemical yield and radiochemical purity without a need for any purification. To further confirm the radiolabeling efficiency, when AGA-1 or AGA-2 (HYNIC precursors) were not added to the labeling solution, only one major peak of [^{99m}Tc]-colloid or [^{99m}Tc]-co-ligand product at 3.3 min was observed, and there was no radioactive peak corresponding to radio-labeled products at 18.0 min or 22.6 min (Figure S1). The specific activity values of the radiotracers were in the range of 540~810 MBq/nmol.

Binding to human AAA tissue

MMP-12 is highly upregulated in human AAA and several preclinical studies have indicated its important role in the development and potentially rupture of AAA.[22, 24, 26, 39, 40] Therefore, as a prelude to performing in vivo imaging studies, we evaluated the binding of ^{99m}Tc-AGA-1 and ^{99m}Tc-AGA-2 to human AAA and normal aorta. Both ^{99m}Tc-AGA-1 & ^{99m}Tc-AGA-2 displayed significantly higher binding to human AAA as compared to normal aortic tissue ($P < 0.001$ for ^{99m}Tc-AGA-1, and $P < 0.001$ for ^{99m}Tc-AGA-2, n = 3 per group, Figure 2).

Radiotracer biodistribution

The biodistribution and blood clearance of ^{99m}Tc-AGA1 and ^{99m}Tc-AGA2 were investigated in C57BL/6J mice following intravenous administration of each radiotracer (18.5 ± 3.7 MBq). These and other animal studies were performed under protocols approved

by Yale University and Veteran Affairs Connecticut institutional animal care and use committees. Serial blood samples were collected over a two-hour period, following which the animals were euthanized and different tissue samples and body fluids were collected, weighed and their radioactivity measured by gamma-well counting. Relative to ^{99m}Tc-AGA-1, ^{99m}Tc-AGA-2 showed faster blood clearance with a residual blood level of 1.2 ± 0.2% injected dose (ID)/mL at 2 h post-injection (p.i.), while the residual blood activity for ^{99m}Tc-AGA-1 was 3.0 ± 0.2% ID/mL at 2 h p.i. (Figure 3). The high activity in bile and kidney indicated a mixed hepato-biliary and renal clearance for both tracers. Importantly, both tracers displayed low uptake (2.0 ± 0.4 and 2.0 ± 0.9 %ID/g, respectively) in the normal aorta, supporting the possibility of using these tracers for vascular imaging applications (Figure 3).

Stability studies

^{99m}Tc-AGA1 and ^{99m}Tc-AGA2 were incubated in murine blood at 37 °C and their stability was monitored by radio-HPLC analysis at 1 and 2 h post-incubation. ^{99m}Tc-AGA1 exhibited poor stability, with the radio-HPLC peak corresponding to the intact tracer decreasing to ~70% of total radioactivity at 1 h and ~50% of that activity at 2 h. Conversely, ^{99m}Tc-AGA2 showed excellent radiochemical stability during the 2 h blood incubation period (Figure 4).

Evaluation in murine model of AAA

Based on its favorable selectivity, pharmacokinetics and stability in blood, ^{99m}Tc-AGA2 was selected for further evaluation in a murine model of AAA that is associated with significant MMP-12 upregulation. Apolipoprotein E deficient (*Apoe*$^{-/-}$) mice (n = 11) were infused with angiotensin (Ang) II (1,000 ng/kg/min; Calbiochem) through a subcutaneous minipump for 4 weeks. As expected, this led to suprarenal AAA development and AAA rupture in a subset of animals.[41] The surviving animals after 4 weeks of Ang II infusion (n = 8), were injected with ^{99m}Tc-AGA2 (37 ± 6 MBq) retro-orbitally under anesthesia, maintained for 1 h post injection. At 2 h post injection, the aorta and carotid arteries were dissected from the surrounding tissues and placed on a phosphor screen (MultiSensitive Phosphor Screen, PerkinElmer) along with standard references of known activity for quantitative autoradiography. The phosphor screen was scanned with a phosphorimager (Typhoon Trio, GE Healthcare Life Sciences) to obtain digitalized images of radiotracer uptake, where focal tracer uptake was readily detectable in animals with AAA (Figure 5). Regions of interest (ROIs) were drawn over different segments of the aorta to quantify the ^{99m}Tc-AGA2 signal (Fiji/ImageJ software, NIH). This showed significantly higher ^{99m}Tc-AGA-2 uptake in the remodeled suprarenal abdominal aorta (srAA), where AAA is typically located, compared to the adjacent, normal size infra-renal abdominal aorta (irAA) (n = 8, $P < 0.01$, paired t test, Figure 5). ^{99m}Tc-AGA-2 in suprarenal aorta was also significantly higher in Ang II-treated animals with AAA than those animals with low remodeling (LR) that had not developed AAA (n=4 in each group, $P < 0.05$, Mann-Whitney U test, Figure 5).

^{99m}Tc-AGA-2 binding specificity

To investigate ^{99m}Tc-AGA-2 binding specificity, we evaluated the effect of MMP inhibitors on tracer binding to AAA and normal size, irAA tissues from Ang II-infused animals, as described above. Co-incubation with 500-fold molar excess of either the panMMP inhibitor,

GM6001, or the MMP-12-specific inhibitor, AGA, significantly reduced ^{99m}Tc-AGA-2 binding to AAA tissue ($P < 0.001$ for both inhibitors) indicating MMP-12-specificity of ^{99m}Tc-AGA-2 binding in AAA (Figure 6). Interestingly, co-incubation with MMP inhibitors had no effect on ^{99m}Tc-AGA-2 binding to irAA tissue, suggesting that the low level of tracer binding to the normal aorta is non-specific (Figure 6).

DISCUSSION AND CONCLUSIONS

Here we report the design, synthesis and preclinical evaluation of first generation of succinate-based hydroxamate analogues as novel selective MMP-12 inhibitors and their ^{99m}Tc labeled HYNIC conjugated analogues as novel MMP-12 selective SPECT radiotracers. Our data show that modifying the P3′-segment of hydroxamate MMP inhibitors with a free acid side chain leads to selective MMP-12 binding. Of the two acyclic MMP-12 tracers developed based on this design, ^{99m}Tc-AGA2 displayed better stability and pharmacokinetics, as well as binding to human and murine AAA tissue. Autoradiography studies confirmed the higher in vivo uptake of the tracer in AAA relative to normal size aorta, setting the stage for future SPECT studies.

MMP-12 plays a key role in several inflammatory diseases such as chronic obstructive pulmonary disease (COPD), atherosclerosis and AAA.[42] Considering the importance of MMP-12 in several pathophysiological processes, this study aimed at developing and evaluating novel selective MMP-12 inhibitors and their corresponding SPECT radiotracers. To date, several panMMP inhibitors and a few selective MMP inhibitors have been reported.[22, 25, 28, 37, 43–46] Amongst these, several are acyclic and macrocyclic hydroxamate analogues which contain a ZBG and a lipophilic side chain at the P1′-segment for interacting with the hydrophobic S1′ pocket of MMPs. Large differences in MMP bindings are observed by changing the side chain at the P1′-segment and hence, the S1′ pocket is considered as the “selectivity pocket”.[47] A few hydroxamate-based MMP inhibitors, e.g., llomasat (GM-6001), RO-32-3555, CGS-27023A, Marimastat, BB-1101, Prinomastat, RO-32-3555, CGS-27023A and Batimastat (BB-94) have been evaluated as therapeutic agents. However, the clinical use of many of these inhibitors is hampered by musculoskeletal toxicity and other side effects, attributed in part to the lack of targeting specificity or selectivity, or the high concentrations of inhibitors required for the therapeutic effects.[19, 48] As an alternative, more selective MMP inhibitors are under development. To access such selective inhibitors, as the structural differences between different MMP family mainly occur at S1′ subsite, the investigators have utilized the P1′ group to introduce the inhibitor specificity.[49, 50] Accordingly, a selective MMP-13 inhibitor has been developed, which is characterized by the absence of catalytic zinc binding site and binding into the S1′ pocket while extending into an additional S1′ side pocket (S1′*).[51] Other investigators have developed thiirane-containing selective MMP-2 and 9 inhibitors, which first coordinate with the active site zinc ion and exploit the deep S1′ pocket of MMP-2 and MMP-9. Considerable MMP-2 selectivity over MMP-9 was also achieved by exploiting the more constricted pocket of MMP-9 than MMP-2 and by introducing a bigger group with unfavorable steric interactions.[52] Phosphinic peptides are known to behave as potent inhibitors of zinc metalloproteases. By exploiting the phosphinic peptide chemistry, a highly selective MMP-12 inhibitor, RXP-470, has been developed.[53]

Succinyl hydroxamate-based small molecules which use the hydroxamate group as their ZBG may be considered as the most successful panMMP inhibitors. However, except for hydroxamate-based selective MMP-2 inhibitors,[54] not much work has been reported on developing single MMP-selective succinyl hydroxamate inhibitors, and specifically, there is no report of selective hydroxamate MMP-12 inhibitors to date. We sought to address this gap by modifying the P3′-segment to achieve selectivity towards a single MMP while maintaining high binding affinities. Accordingly, several succinyl hydroxamate analogues, i.e., CGA, CGA-1, AGA, AGA-1 and AGA-2 were designed and successfully synthesized by incorporating an acid side chain within the P3′-segment. The macrocyclic hydroxamate MMP-12 inhibitors, CGA & CGA-1, were synthesized starting from anti-succinate derivatives, following a synthetic strategy reported previously with some modifications.[33] The synthesis of the intermediate **7** was achieved according to the literature and coupling of *o*-benzyl hydroxamate to the free acid followed by de-protection of both benzyl groups resulted in CGA. To synthesize CGA-1, a di-protected glutamate was added to CGA, followed by de-protection of both ester groups. The strategy used for the synthesis of the acyclic AGA followed a previously reported synthetic methodology with modifications.[36] The intermediate **15** was synthesized starting from 4-methylvaloric acid and s-4-benzyl-2-oxazolidinone. The hydrolysis of ester and coupling of *o*-benzyl hydroxamate to the free acid followed by de-protection of both benzyl groups resulted in AGA. AGA-1 was synthesized using a multi-protected glutamate with a selective de-protection strategy and addition of HYNIC at the end, as shown above. AGA-2 was synthesized by replacing the phenylalanine ester from the AGA synthetic scheme with L-tyrosine benzyl ester. The HYNIC group was added by functionalizing the hydroxyl group on the phenyl to generate a free amine, which in turn was coupled to a HYNIC acid to obtain AGA-2 through peptide coupling. The synthetic strategy introduced here is novel for this class of anti-succinate hydroxamate derivatives, where the P2′ position was used for adding a HYNIC group (a chelator for ^{99m}Tc-radiolabeling). This synthetic strategy reduced the number of synthetic steps (8 vs 13 for AGA1 and AGA2, respectively), increasing the yields and feasibility of synthesis. Also, this synthetic strategy allowed us to keep the free acid on P3′ position, which resulted in better MMP-12 binding selectivity than AGA-1.

All these molecules with an acid side chain in their C-terminal end displayed selective nanomolar inhibition towards rhMMP-12. When both acid groups on the side chain of CGA-1 were replaced by amide groups, the resulting molecule (RYM) lost its selectivity towards MMP-12 and displayed nanomolar inhibition towards all the rhMMPs tested. Hence, it is understood that the presence of an acid side chain around the P3′-segment of succinyl hydroxamate analogues is one of the key reasons for achieving MMP-12 selectivity. Such an impact was rather unexpected in hydroxamate series but was however consistent with previous observations made on MMP-12 selective inhibitors for which two glutamate residues in P3’ and P2’ position induce a favorable MMP-12 selectivity profile.[35, 53] Since the analysis of the crystal structure of those inhibitors in interaction with MMP-12 did not reveal any specific interaction of glutamate residues within the catalytic cleft, it was postulated that the MMP-12 selectivity of those inhibitors was more likely related to the presence of two negative charges, better tolerated in the case of MMP-12 than in that of other tested MMPs. In any event, the presence of a carboxylic function in the C-ter end of

inhibitors described in the present study has significant effects on their selectivity profile but several other structural differences must be considered. Accordingly, the ring opening from cyclic CGA to acyclic AGA inhibitor has almost no impact on binding to MMP-2 and MMP-13 while a drop in potency (10 fold) is observed for MMP-7 and 12. Interestingly, further structural modifications on the AGA scaffold (AGA-1 and 2) have no effect on binding to MMP-12 but impact in variable extent the inhibitors potency toward other MMPs tested. Particularly, the position of the bulky HYNIC moiety relative to the pseudo peptide backbone seemed to have major effects on inhibitors binding, with a conjugation of this group onto the P2' side chain that was particularly well tolerated by MMP-12 while rejected by MMP-2/7 and 13. Overall, AGA2 that both combined a carboxylic function in its C-ter end and an HYNIC moiety in its P2' position appeared to be the most selective agent amongst the set of inhibitors designed in this study.

HYNIC, along with two co-ligands such as TPPTS and tricine, is a widely used chelator for ^{99m}Tc-labeling. Importantly, AGA and its HYNIC conjugated radiolabeling precursors, AGA-1 and AGA-2, displayed a selective inhibition profile towards MMP-12. This demonstrated that adding a HYNIC moiety does not have a significant effect on MMP-12 binding and inhibition. This confirmed previous results, with a C-ter extension on the pseudo peptide scaffold that did not significantly impact the MMP-12 selectivity profile of optical probes or radiotracers compared to their parent molecule.[40, 55, 56] Both AGA-1 & AGA-2 were conveniently radiolabeled with ^{99m}Tc using TPPTS and tricine formulation in high radiochemical purity and yield to access ^{99m}Tc-AGA1 and ^{99m}Tc-AGA2.

MMP-12 gene expression is significantly upregulated in human AAA and both ^{99m}Tc-AGA1 and ^{99m}Tc-AGA2 displayed higher binding to human AAA than normal aortic tissue. The stability studies performed in murine blood revealed that ^{99m}Tc-AGA-1 is not stable and disintegrates over time, whereas ^{99m}Tc-AGA-2 was found stable at least for 2 h. From the bio distribution studies, we found that tracer ^{99m}Tc-AGA-2 clears faster from the blood when compared to ^{99m}Tc-AGA-1 (1.2 ± 0.2 and 3.0 ± 0.2 %ID/mL respectively). Based on favorable blood kinetics and stability in murine blood, ^{99m}Tc-AGA-2 was chosen for further evaluation. For preclinical evaluation of our new tracers, we used an established animal model of AAA with significant upregulation of MMP-12 in aneurysm, i.e., *Apoe*$^{-/-}$ mice infused with Ang II.[41] In vivo evaluation of ^{99m}Tc-AGA-2 in Ang II-infused mice revealed significantly higher tracer uptake in AAA, where MMP-12 expression is upregulated. Blocking experiments with panMMP and MMP-12 inhibitors performed with mouse tissues established the MMP-12 specific binding of ^{99m}Tc-AGA-2 in AAA by reducing tracer binding in AAA to the non-specific low levels observed in normal aortae. Combined, these data support the potential of ^{99m}Tc-AGA-2 for molecular imaging of MMP-12 activation, not only in AAA, but also other diseases that are associated with MMP-12 upregulation.

In conclusion, this study reports the development and evaluation of novel succinyl hydroxamate-based selective MMP-12 inhibitors and their corresponding ^{99m}Tc-labeled radiotracers. MMP-12 selectivity was achieved by introducing an acid around the P3′-segment of succinyl hydroxamate analogues. The lead tracer, ^{99m}Tc-AGA-2, has favorable pharmacokinetics for vascular imaging and binds selectively to murine AAA in vivo. This

sets the stage for future in vivo SPECT imaging studies in AAA and other inflammatory diseases where MMP-12 plays a key role.

EXPERIMENTAL SECTION

Commercially available reagents and solvents were purchased from Sigma-Aldrich (USA) and used as received without further purification. The following instruments were used for quality control; (1) HPLC: Waters HPLC system 2489, UV-Vis detector, 600 controller, and Empower Pro sofware. (2) LC-MS: Agilent LC-MS 6120B Quadrupole, 6550A iFunnel Q-TOF. (3) HRMS: Agilent QToF 6546 instrument (over 30,000 resolution at ~200mw) was used with gradual increase in buffer composition 0% – 80% MeOH in water in 10 mins. (4) NMR: Agilent NMR DD2 400MHz with OneProbe (Agilent Technologies, Santa Clara, CA, USA). (5) Fluorescent plate reader (BIO-TEK/ Synergy HT). The identity and purity of the final compounds and key intermediates were assessed by analytical HPLC (see supplemental information for representative chromatograms), HRMS & ^{1}H NMR (see supplemental information for representative HRMS & NMR spectra). Each final compound displayed a purity >95%.

Synthetic Chemistry:

Intermediate 6: 1 g (1.65 mmol) of **5** was dissolved in 20mL of acetonitrile and 1.9 g (5.96 mmol) of Cs_2CO_3 was added and stirred at room temperature for 6 h. The solution was concentrated, added 50 mL of water and extracted with ethyl acetate (50 mL × 3). The combined organic layers were dried over $MgSO_4$, filtered, concentrated and purified by flash column chromatography to give 460 mg (55 %) of the title compound. ES-MS: Observed $[MH]^+$ 524.2 ^{1}H NMR (400 MHz, Chloroform-*d*) δ 7.99 (dt, 1H), 7.62 – 7.47 (m, 2H), 7.43 – 7.28 (m, 6H), 7.02 – 6.91 (m, 2H), 6.80 – 6.71 (m, 2H), 6.05 (d, 1H), 5.24 – 4.93 (m, 3H), 4.47 – 4.26 (m, 2H), 3.18 (dd, 1H), 3.04 – 2.78 (m, 3H), 2.35 (dtd, 2H), 1.77 – 1.61 (m, 3H), 1.42 (s, 10H), 1.15 (dtd, 1H), 1.00 (ddd, 1H), 0.81 (dd, 6H) (Figure S2).

Intermediate 7: 250 mg of **6** was dissolved in 4mL TFA and 1mL DCM. After stirred at room temperature for 2 h, the solution was concentrated and dried under vacuum to get the title compound in a quantitative yield. ES-MS: Observed $[MH]^+$ 468.2.

Intermediate 8: A mixture of **7 (**220 mg, 0.47 mmol), (2-(1*H*-benzotriazol-1-yl)-1,1,3,3-tetramethyluronium hexafluorophosphate (HBTU) (214 mg, 0.56 mmol) and DIEA (0.4 mL, 2.35 mmol) was dissolved in 2.5 mL anhydrous DMF. The mixture was stirred at room temperature for 20 min, followed by adding Bn-ONH_2 (247.0 mg, 1.55 mmol). The mixture was further stirred at room temperature for 18 h. 25 mL of cold H2O was added, stirred and filtered the solid formed. The solid was vacuum dried and used for next step. Yield 165 mg (62 %), ES-MS: Observed $[MH]^+$ 573.2. ^{1}H NMR (400 MHz, Chloroform-*d*) δ 7.60 – 7.28 (m, 10H), 6.95 (dt, 2H), 6.81 – 6.67 (m, 2H), 5.32 – 4.94 (m, 4H), 4.51 – 4.32 (m, 2H), 3.53 – 3.32 (m, 2H), 2.43 – 2.24 (m, 2H), 1.87 – 1.47 (m, 6H), 1.47 – 1.30 (m, 2H), 1.22 – 0.98 (m, 1H), 0.86 (td, 6H) (Figure S3).

Intermediate 9 (CGA): A mixture of **8** (100 mg, 0.17 mmol) and Pd/C (0.02 g, 20%, wet) in 10 mL methanol was stirred under hydrogen gas at room temperature for 2 h. The mixture

was filtered, followed by washing the Pd/C with methanol (5 mL × 4). The combined methanol filtrate was concentrated, and the product was further purified by flash column chromatography to give 40 mg (58 %) of the title compound. ES-MS: Observed $[M-H]^-$ 391.2. ^{1}H NMR (400 MHz, DMSO-d_6) δ 10.33 (s, 1H), 8.67 (s, 1H), 7.73 (d, 1H), 7.21 – 6.96 (m, 3H), 6.79 (dd, 1H), 4.70 (s, 1H), 4.09 (s, 3H), 2.07 – 1.91 (m, 1H), 1.69 – 1.55 (m, 1H), 1.39 – 1.10 (m, 4H), 0.89 – 0.66 (m, 6H) (Figures S4 and S5).

Intermediate 10: To a stirred solution of **9** (30 mg, 0.07 mmol) in 1 mL anhydrous DMF was added EDCI (30 mg, 0.157 mmol), HOBT (22 mg, 0.157 mmol), L-glutamic acid di-*tert*-butyl ester (40 mg, 0.157 mmol) and stirred at room temperature for overnight. To the resulting mixture ice cold water (100 mL) was added and stirred for 30 min. The resulting solid was filtered, dried and purified by chromatography (silica gel, 5% methanol/DCM) to obtain 12 mg (25%) of the title compound. ES-MS: Observed $[MH]^+$ 634.2

Intermediate 11 (CGA-1): A mixture of **10** (12 mg, 0.018 mmol) in 100 mL of DCM was cooled to 0 °C and added 20mL of TFA dropwise. The mixture was stirred for 2 h at room temperature and concentrated under vacuum to remove solvent and excess TFA. The reaction mixture was further dried by co-distilling with Toluene twice (10 mL × 2) and purified by prep HPLC. ES-MS: Observed $[M-H]^-$ 520.2. ^{1}H NMR (400 MHz, DMSO-d_6) δ 10.34 (s, 1H), 8.68 (s, 1H), 7.92 (d, 1H), 7.51 (d, 1H), 7.29 – 6.97 (m, 3H), 6.82 (dd, 1H), 6.56 (s, 1H), 4.74 (ddd, 1H), 4.28 – 3.92 (m, 4H), 2.27 (q, 2H), 2.00 (td, 1H), 1.92 – 1.75 (m, 2H), 1.60 (td, 1H), 1.44 – 1.04 (m, 4H), 0.89 – 0.53 (m, 6H) (Figure S6 and S7).

Intermediate 16: 500 mg of **15** was dissolved in 4mL TFA and 5mL DCM. After stirred at room temperature for 2 h, the solution was concentrated and dried under vacuum to get the title compound in a quantitative yield. ES-MS: Observed $[MH]^+$ 412.2.

Intermediate 17: A mixture of **16 (**180 mg, 0.42 mmol), **b**enzotriazol-1-yl**o**xytris(dimethylamino)**p**hosphonium hexafluorophosphate (BOP) (0.22 g, 0.506 mmol) and DIEA (290 mg, 1.68 mmol) was dissolved in 4 mL anhydrous DMF. The mixture was stirred at room temperature for 20 min, followed by adding Bn-ONH_2 (62 mg, 0.506 mmol). The mixture was further stirred at room temperature overnight and concentrated. The residue was triturated with 1 N HCl, the solid obtained was filtered, and washed with 1 N Na_2CO_3, water and brine. The product was further purified by flash column chromatography to give 180 g (80 %) of the title compound. ES-MS: Observed $[MH]^+$ 517.2

Intermediate 18 (AGA): A mixture of **17** (100 mg, 0.193 mmol) and Pd/C (0.01 g, 10%, wet) in 10 mL methanol was stirred under hydrogen gas at room temperature for 2 h. The mixture was filtered, followed by washing the Pd/C with methanol (5 mL × 4). The combined methanol filtrate was concentrated, and the product was further purified by flash column chromatography to give 40 mg (62 %) of the title compound. ES-MS: Observed $[M-H]^-$ 335.1. Representative NMR & HRMS spectra are shown in the supporting information. ^{1}H NMR (400 MHz, Methanol-d_4) δ 7.35 – 7.16 (m, 5H), 4.75 – 4.62 (m, 1H), 3.21 (dd, 1H), 3.10 – 2.94 (m, 1H), 2.94 – 2.74 (m, 1H), 2.05 (qd, 2H), 1.53 (ddt, 2H), 1.11 (ddt, 1H), 0.88 (dd, 6H) (Figure S8 and S9).

Intermediate 19: To a stirred solution of Fmoc-Glu(O-Bn)-OH (2.0 g, 4.35 mmol), HOBT (0.7 g, 5.22 mmol), and N-Boc-ethylenediamine (0.77 g, 4.79 mmol) in 20mL anhydrous DMF cooled in an ice bath, was added EDCI (1 g, 5.224 mmol) and stirred at room temperature for 2.5 h. Ice cold water was added to the resulting mixture, stirred and filtered the solid obtained. The resulting residue was purified by chromatography (silica gel, 60% ethyl acetate/hexane). 1.8 g (72%) of the title compound was obtained. ES-MS: Observed $[MH]^+$ 602.2. ^{1}H NMR (400 MHz, Chloroform-*d*) δ 7.81 – 7.60 (m, 2H), 7.51 (d, 2H), 7.38 – 7.18 (m, 9H), 5.11 – 4.97 (m, 2H), 4.33 (q, 2H), 4.13 (t, 2H), 3.43 – 3.04 (m, 4H), 2.57 – 2.26 (m, 2H), 2.20 – 1.99 (m, 1H), 2.00 – 1.82 (m, 1H), 1.34 (s, 9H) (Figure S10).

Intermediate 20: 1.0 g of **19** obtained above was dissolved in 10 mL DCM and 3 mL piperidine. The mixture was stirred at room temperature for 30 min and concentrated under vacuum. The product was purified by flash column chromatography (2% Methanol/DCM) to give the title compound (0.6 g, 72%). ES-MS: Observed $[MH]^+$ 502.2. ^{1}H NMR (400 MHz, Methanol-d_4) δ 7.91 – 7.53 (m, 5H), 7.49 – 7.20 (m, 8H), 5.14 (s, 2H), 4.53 – 4.40 (m, 1H), 4.37 (dd, 1H), 4.24 (dt, 1H), 4.09 (dd, 1H), 3.59 – 3.37 (m, 3H), 3.17 – 2.94 (m, 2H), 2.44 (dt, 2H), 2.22 – 2.04 (m, 1H), 2.05 – 1.86 (m, 1H) (Figure S11).

Intermediate 21: To a stirred solution of **20** (100 mg, 0.2 mmol) in 1 mL anhydrous DMF was added EDCI (40 mg, 0.24 mmol), HOBT (32 mg, 0.24 mmol), 6-Boc-hydrazinonicotinic acid (50 mg, 0.2 mmol) and stirred at room temperature for overnight. To the resulting mixture ice cold water (100 mL) was added and stirred for 30 min. The resulting solid was filtered, dried and purified by chromatography (silica gel, 1% methanol/DCM) to obtain 80 mg (55%) of the title compound. ES-MS: Observed $[MH]^+$ 737.2. ^{1}H NMR (400 MHz, DMSO-d_6) δ 8.99 – 8.80 (m, 1H), 8.52 – 8.35 (m, 2H), 8.24 (s, 1H), 8.00 – 7.84 (m, 2H), 7.79 (d, 2H), 7.63 (t, 2H), 7.49 – 7.38 (m, 1H), 7.37 – 7.15 (m, 9H), 6.52 (dd, 1H), 4.99 (s, 2H), 4.31 – 4.06 (m, 3H), 3.90 (td, 1H), 2.47 (d, 7H), 2.29 (t, 2H), 1.87 (ddd, 1H), 1.79 – 1.64 (m, 1H), 1.33 (s, 9H) (Figure S12).

Intermediate 22: 80 mg of **21** obtained above was dissolved in 10 mL DCM and 3 mL piperidine. The mixture was stirred at room temperature for 30 min and concentrated under vacuum. The product was purified by flash column chromatography (2% Methanol/DCM) to give the title compound (35 mg, 65%). ES-MS: Observed $[MH]^+$ 515.2. ^{1}H NMR (400 MHz, Methanol-d_4) δ 8.55 (dd, 2H), 8.27 – 8.12 (m, 1H), 8.02 (dd, 1H), 7.44 – 7.27 (m, 2H), 6.71 (dd, 2H), 4.17 (dd, 2H), 3.72 – 3.37 (m, 9H), 2.59 – 2.20 (m, 7H), 2.18 – 2.00 (m, 3H), 1.50 (s, 9H) (Figure S13).

Intermediate 23: A mixture of **18 (**20 mg, 0.06 mmol), **22** (37 mg, 0.07 mmol), and HOBT (10 mg, 0.07 mmol) were dissolved in 2 mL DMF and cooled at 0~5°C in an ice bath, followed by adding EDCI (14 mg, 0.07 mmol). The mixture was stirred at room temperature overnight and concentrated. The residue was dissolved in 10 mL CH_2Cl_2, washed with 1N HCl, H_2O, and brine. The DCM solution was dried over $MgSO_4$, filtered, and concentrated. The product was purified by flash column chromatography (2% methanol/DCM) to give the title compound (21 mg, 45%). ES-MS: Observed $[MH]^+$ 799.9.

Intermediate 24 (AGA-1): 20 mg of **23** was dissolved in 2mL TFA and 1mL DCM. After stirred at room temperature for 2 h, the solution was concentrated and dried under vacuum to get crude t-butyl deprotected acid product. To the acid, Pd/C (4 mg, 20%, wet) in 1 mL methanol was stirred under hydrogen gas at room temperature for 2 h. The mixture was filtered, followed by washing the Pd/C with methanol (1 mL × 4). The combined methanol filtrate was concentrated, and the product was further purified by flash column chromatography followed by preparative HPLC purification to give 2 mg (14 %) of the title compound. ES-MS: Observed $[MH]^+$ 643.3. ^{1}H NMR (400 MHz, Chloroform-*d*) δ 7.38 – 7.19 (m, 6H), 6.80 (d, 2H), 6.69 – 6.47 (m, 2H), 5.20 – 4.88 (m, 2H), 4.74 (d, 3H), 2.99 (dd, 2H), 2.84 (dd, 2H), 2.65 (tt, 2H), 2.11 (ddd, 2H), 1.41 (q, 2H), 1.30 – 1.12 (m, 2H), 1.02 (ddd, 1H), 0.71 (m, 6H) (Figure S14 and S15).

Intermediate 27: A mixture of **26 (**2 g, 4.7 mmol), (2-(1*H*-benzotriazol-1-yl)-1,1,3,3-tetramethyluronium hexafluorophosphate (HBTU) (2.14 g, 5.6 mmol) and DIEA (1.6 mL, 9.4 mmol) was dissolved in 20 mL anhydrous DMF. The mixture was stirred at room temperature for 20 min, followed by adding Bn-ONH_2 (988 mg, 6.2 mmol). The mixture was further stirred at room temperature for 18 h. 250 mL of cold H2O was added, stirred and filtered the solid formed. The solid was vacuum dried and used for next step. Yield 1.65 g (66 %), ES-MS: Observed $[MH]^+$ 533.6. ^{1}H NMR (400 MHz, Methanol-d_4) δ 7.47 – 7.25 (m, 9H), 7.08 – 6.94 (m, 2H), 6.77 – 6.59 (m, 2H), 5.10 (d, 2H), 4.90 – 4.74 (m, 7H), 4.65 (dd, 1H), 3.12 – 2.75 (m, 3H), 2.23 – 1.90 (m, 2H), 1.56 – 1.36 (m, 2H), 1.09 – 1.00 (m, 1H), 0.83 (dd, 6H) (Figure S16).

Intermediate 28: To a stirred solution of 2-(BOC-amino)ethyl bromide (0.31 g, 1.4 mmol), Cs_2CO_3 (0.92 g, 2.82 mmol) in 10 mL anhydrous acetonitrile at 60 °C, was added dropwise a solution of **27** (0.5 g, 0.94 mmol) in 5 mL acetonitrile, over a period of 1 h. The resulting mixture was stirred at 60 °C for another 3 h and concentrated under vacuum. The product was re-dissolved with ethyl acetate and filtered, followed by washing the solid with ethyl acetate for 5 times (10 mL × 5). The combined ethyl acetate filtrate was washed with 1 N HCl solution, water, and brine. The ethyl acetate solution was dried over anhydrous $MgSO_4$, filtered, and concentrated. The resulting residue was purified by silica gel chromatography using (silica gel, 40% ethyl acetate/hexane) to give the product (0.4 g, 58%). ES-MS: observed $[MH]^+$ 676.3. ^{1}H NMR (400 MHz, DMSO-d_6) δ 7.47 – 7.18 (m, 10H), 7.15 – 7.08 (m, 1H), 7.03 – 6.93 (m, 1H), 6.87 – 6.71 (m, 1H), 6.67 – 6.62 (m, 1H), 5.18 – 4.96 (m, 2H), 4.90 – 4.67 (m, 2H), 4.51 – 4.37 (m, 1H), 3.87 (td, 1H), 3.11 (d, 1H), 3.01 – 2.82 (m, 2H), 2.78 (d, 1H), 1.38 (s, 9H), 1.14 – 1.05 (m, 1H), 0.86 – 0.68 (m, 6H) (Figure S17).

Intermediate 29: 400 mg of **28** was dissolved in 4 mL TFA and 6 mL DCM. After stirred at room temperature for 2 h, the solution was concentrated and dried under vacuum to get crude boc-deprotected free amine product in quantitative amounts, which was used directly for next step. ES-MS: observed $[MH]^+$ 576.3.

Intermediate 30: To a stirred solution of **29** (100 mg, 0.174 mmol) in 5 mL anhydrous DMF was added 1-hydroxy-7-azabenzotriazole (HOAt) (47 mg, 0.35 mmol),

hexafluorophosphate azabenzotriazole tetramethyl uronium (HATU) (132 mg, 0.38 mmol), 6-Boc-hydrazinonicotinic acid (88 mg, 0.35 mmol) and stirred at room temperature for overnight. To the resulting mixture ice cold water (50 mL) was added and stirred for 30 min. The resulting solid was filtered, dried and purified by chromatography (silica gel, 1% methanol/DCM) to obtain 74 mg (53%) of the title compound. ES-MS: Observed $[MH]^+$ 737.2. ^{1}H NMR (400 MHz, DMSO-d_6) δ 8.96 – 8.28 (m, 8H), 8.01 – 7.73 (m, 3H), 7.48 – 7.03 (m, 12H), 6.83 (d, J = 8.6 Hz, 2H), 6.51 (t, J = 9.5 Hz, 2H), 5.13 – 4.93 (m, 3H), 4.70 (d, J = 2.9 Hz, 2H), 4.45 (q, J = 7.5, 7.0 Hz, 2H), 4.04 (t, J = 5.9 Hz, 5H), 3.80 (d, J = 7.8 Hz, 6H), 3.09 (d, J = 7.4 Hz, 2H), 2.92 (dd, J = 11.9, 7.3 Hz, 3H), 2.72 (s, 2H), 2.06 (tt, J = 14.5, 5.8 Hz, 3H), 1.45 – 1.35 (m, 11H), 0.85 – 0.60 (m, 6H) (Figure S18).

Intermediate 31: 50 mg of **30** was dissolved in 1 mL TFA and 2 mL DCM. After stirred at room temperature for 2 h, the solution was concentrated and dried under vacuum to get crude boc-deprotected free amine product in quantitative amounts, which was used directly for next step. ES-MS: observed $[MH]^+$ 637.2

Intermediate 32 (AGA-2): A mixture of **31** (40 mg, 0.193 mmol) and Pd/C (0.01 g, 25%, wet) in 4 mL methanol was stirred under hydrogen gas at room temperature for 2 h. The mixture was filtered, followed by washing the Pd/C with methanol (5 mL × 4). The combined methanol filtrate was concentrated, and the product was further purified by flash column chromatography and preparative HPLC to give 2.9 mg (9 %, after two steps) of the title compound. ES-MS: Observed $[MH]^+$ 530.7. ^{1}H NMR (400 MHz, Methanol-d_4) δ 8.53 – 8.35 (m, 2H), 7.99 – 7.79 (m, 2H), 7.04 (dq, J = 7.0, 3.3 Hz, 2H), 6.82 – 6.67 (m, 2H), 6.58 (dd, J = 8.8, 6.3 Hz, 2H), 3.99 (p, J = 5.5 Hz, 2H), 3.78 – 3.54 (m, 3H), 3.39 (q, J = 7.0 Hz, 2H), 3.02 (d, J = 4.8 Hz, 1H), 2.87 – 2.75 (m, 1H), 2.65 (s, 1H), 2.23 – 1.93 (m, 2H), 0.86 – 0.56 (m, 6H) (Figure S19 and S20).

MMP affinity determination

The MMP inhibition constants for newly synthesized MMP-12 selective inhibitors were measured based on the kinetic effects of an inhibitor on MMP-mediated catalytic cleavage of a fluorogenic substrate, namely Mca-Lys-Pro-Leu-Gly-Leu-Dpa-Ala-Arg-NH_2, in an assay buffer of 50 mM Tris/HCl buffer, pH 6.8, 10 mM $CaCl_2$ at 25 °C. The inhibition constants were measured towards MMP-2, 7, 9, 12 and 13, using 0.2–0.5 nM of the MMP, at 4 different concentrations of the fluorogenic substrate (8 μM, 16 μM, 32 μM & 64 μM) and at 5 different concentrations of the inhibitors (31.25 nM, 125 nM, 0.5 μM, 2.5 μM, 5 μM). The assays were performed in black flat-bottomed 96-well plates (Microfluor 1 Black, Thermo Fisher Scientific). The fluorescence signals were monitored using a BIO-TEK synergy HT spectrophotometer equipped with a plate shaker and temperature device controller. From the fluorescence measured, the Ki values were determined using the method previously proposed by Horovitz and Leviski.[57]

Radiolabeling

^{99m}Tc-labeling of precursors AGA1 and AGA2 was performed according to an established methodology.[37, 38] Briefly, the co-ligand kits for radiolabeling of HYNIC precursors with $^{99m}TcO_4^-$ were prepared by lyophilizing the solution containing tricine (6.5 mg/ml),

3,3′,3″-phosphanetriyltris(benzenesulfonic acid) trisodium salt (TPPTS) (5.0 mg/ml), pluronic F-127 (0.1 mg/ml), succinic acid (12.7 mg/ml), sodium succinate (38.5 mg/ml) and Mannitol (40 mg/ml).[33] Each kit was mixed with 2 μg (in 2 μL DMSO) of HYNIC precursor (AGA-1 or AGA-2), and 200–400 μL (740–1110 MBq) of $^{99m}TcO_4^-$solution and heated at 95 °C for 20 min. The radio-labeled solution was cooled down to room temperature before subjecting it to quality control by instant thin layer chromatography (ITLC) and radio high performance liquid chromatography (HPLC) analysis. ITLC analysis was performed using either silica gel plate or TLC paper as stationary phase and acetonitrile as mobile phase. HPLC analysis was performed using C-18 reverse-phase analytical column as stationary phase and aqueous acetonitrile (containing 0.16% ammonium formate) and water (containing 0.16% ammonium formate) as mobile phase for gradient elution.

Tracer binding to human tissues

Human tissues were collected from anonymous donors under a protocol approved by Yale University institutional review board (#12481). Frozen tissue sections of human AAA and normal aorta were incubated in triplicates with ~ 1.8 MBq of ^{99m}Tc-AGA-1 or ^{99m}Tc-AGA-2 at 37 °C for 2 h. Following washing away the unbound radiotracer, the bound activity in each sample was measured using a gamma counter (WIZARD2, PerkinElmer). Next, 200 μL of protein lysis buffer (NaCl 0.3 M, Tris 50 mM, Triton X-100 1%, cOmplete Protease Inhibitor Cocktail [SigmaAldrich]), was added to each sample, aortic tissue was lysed and protein concentration was measured using a colorimetric assay (Protein Assay Dye Reagent Concentrate [Bio-Rad], BioMate 3 [Thermo Scientific]). The bound activity in each sample was normalized to protein concentration.

Supplementary Material

Refer to Web version on PubMed Central for supplementary material.

ACKNOWLEDGEMENTS

This work was supported by NIH grant R01HL138567 and VA Merit grant I01BX004038. PB and MS were supported by NIH training grants (5T32HL98069 and 5T32HL007950). We thank Dr. Mousumi Ghosh for assistance in chemical analyses. The resources of the Yale Translational Research Imaging Center, funded in part by NIH grant 1S10RR018039, and West Campus Analytical Core at Yale University were used for these studies.

Abbreviations Used

AAA	abdominal aortic aneurysm
ECM	extracellular matrix
TIMP	tissue inhibitors of metalloproteinases
srAA	suprarenal abdominal aorta
irAA	infrarenal abdominal aorta
ZBG	zinc binding group
EDC-I	1-Ethyl-3-(3-dimethylaminopropyl) carbodiimide

HOBT	1-Hydroxybenzotriazole hydrate
RT	room temperature
pivCl	pivaloyl chloride
BOP	benzotriazol-1-yloxytris(dimethylamino)phosphonium hexafluorophosphate
DIEA	N,N-diisopropylethylamine
HATU	hexafluorophosphate azabenzotriazole tetramethyl uranium
HOAT	1-hydroxy-7-azabenzotriazole
rh	recombinant human
Bq	becquerel
ID	injected dose
Ang II	angiotensin II
ROI	region of interest
TPPTS	3,3′,3″-phosphanetriyltris(benzenesulfonic acid) trisodium salt
HYNIC	6-hydrazinonicotinyl

REFERENCES

1. Nagase H Zinc metalloproteases in health and disease. London: Taylor & Francis 1996, 153–204.
2. Paiva KBS; Granjeiro JM Bone tissue remodeling and development: focus on matrix metalloproteinase functions. Archives of biochemistry and biophysics 2014, 561, 74–87. [PubMed: 25157440]
3. Tomlinson ML; Garcia-Morales C; Abu-Elmagd M; Wheeler GN Three matrix metalloproteinases are required in vivo for macrophage migration during embryonic development. Mechanisms of Development 2008, 125, 1059–1070. [PubMed: 18684398]
4. Werb Z; Chin JR Extracellular Matrix remodeling during morphogenesisa. Annals of the New York academy of sciences 1998, 857, 110–118. [PubMed: 9917836]
5. Bottomley K; Johnson W; Walter D Matrix metalloproteinase inhibitors in arthritis. Journal of enzyme inhibition 1998, 13, 79–101. [PubMed: 9629530]
6. Jabłońska-Trypuć A; Matejczyk M; Rosochacki S Matrix metalloproteinases (MMPs), the main extracellular matrix (ECM) enzymes in collagen degradation, as a target for anticancer drugs. Journal of Enzyme Inhibition and Medicinal Chemistry 2016, 31, 177–183. [PubMed: 27028474]
7. Kuzuya M; Nakamura K; Sasaki T; Wu Cheng X; Itohara S; Iguchi A Effect of MMP-2 deficiency on atherosclerotic lesion formation in apoE-deficient mice. Arteriosclerosis, thrombosis, and vascular biology 2006, 26, 1120–1125.
8. Li H; Simon H; Bocan TM; Peterson JT MMP/TIMP expression in spontaneously hypertensive heart failure rats: the effect of ACE-and MMP-inhibition. Cardiovascular research 2000, 46, 298–306. [PubMed: 10773234]
9. Nygårdas P; Hinkkanen A Up-regulation of MMP-8 and MMP-9 activity in the BALB/c mouse spinal cord correlates with the severity of experimental autoimmune encephalomyelitis. Clinical & Experimental Immunology 2002, 128, 245–254. [PubMed: 11985514]

10. Rayment EA; Upton Z; Shooter GK Increased matrix metalloproteinase-9 (MMP-9) activity observed in chronic wound fluid is related to the clinical severity of the ulcer. British Journal of Dermatology 2008, 158, 951–961.
11. Steinmann-Niggli K; Ziswiler R; Küng M; Marti H-P Inhibition of matrix metalloproteinases attenuates anti-Thy1. 1 nephritis. Journal of the American Society of Nephrology 1998, 9, 397–407. [PubMed: 9513901]
12. Van Linthout S; Seeland U; Riad A; Eckhardt O; Hohl M; Dhayat N; Richter U; Fischer JW; Böhm M; Pauschinger M Reduced MMP-2 activity contributes to cardiac fibrosis in experimental diabetic cardiomyopathy. Basic research in cardiology 2008, 103, 319–327. [PubMed: 18347835]
13. Lee R; Kermani P; Teng KK; Hempstead BL Regulation of cell survival by secreted proneurotrophins. Science 2001, 294, 1945–1948. [PubMed: 11729324]
14. Van Lint P; Libert C Chemokine and cytokine processing by matrix metalloproteinases and its effect on leukocyte migration and inflammation. J Leukoc Biol 2007, 82, 1375–1381. [PubMed: 17709402]
15. Yamamoto M; Hirayama R; Naruse K; Yoshino K; Shimada A; Inoue S; Kayagaki N; Yagita H; Okumura K; Ikeda S Structure-activity relationship of hydroxamate-based inhibitors on membrane-bound Fas ligand and TNF-alpha processing. Drug Des Discov 1999, 16, 119–130. [PubMed: 10533808]
16. Hu J; Van den Steen PE; Sang Q-XA; Opdenakker G Matrix metalloproteinase inhibitors as therapy for inflammatory and vascular diseases. Nature Reviews Drug Discovery 2007, 6, 480–498. [PubMed: 17541420]
17. Cawston TE Metalloproteinase inhibitors and the prevention of connective tissue breakdown. Pharmacol Ther 1996, 70, 163–182. [PubMed: 8888065]
18. Liedtke W; Cannella B; Mazzaccaro RJ; Clements JM; Miller KM; Wucherpfenning KW; Gearing AJH; Raine CS Effective treatment of models of multiple sclerosis by matrix metalloproteinase inhibitors. Annals of Neurology 1998, 44, 35–46. [PubMed: 9667591]
19. Winer A; Adams S; Mignatti P Matrix metalloproteinase inhibitors in cancer therapy: Turning past failures into future successes. Molecular Cancer Therapeutics 2018, 17, 1147–1155. [PubMed: 29735645]
20. Golestani R; Razavian M; Ye Y; Zhang J; Jung JJ; Toczek J; Gona K; Kim HY; Elias JA; Lee CG; Homer RJ; Sadeghi MM Matrix metalloproteinase-targeted imaging of lung inflammation and remodeling. J Nucl Med 2017, 58, 138–143. [PubMed: 27469361]
21. Matusiak N; van Waarde A; Bischoff R; Oltenfreiter R; van de Wiele C; Dierckx RA; Elsinga PH Probes for non-invasive matrix metalloproteinase-targeted imaging with PET and SPECT. Curr Pharm Des 2013, 19, 4647–4672. [PubMed: 23339739]
22. Toczek J; Ye Y; Gona K; Kim HY; Han J; Razavian M; Golestani R; Zhang J; Wu TL; Jung JJ; Sadeghi MM Preclinical evaluation of RYM1, a matrix metalloproteinase-targeted tracer for imaging aneurysm. J Nucl Med 2017, 58, 1318–1323. [PubMed: 28360209]
23. Lagente V; Le Quement C; Boichot E Macrophage metalloelastase (MMP-12) as a target for inflammatory respiratory diseases. Expert Opinion on Therapeutic Targets 2009, 13, 287–295. [PubMed: 19236151]
24. Longo GM; Buda SJ; Fiotta N; Xiong W; Griener T; Shapiro S; Baxter BT MMP-12 has a role in abdominal aortic aneurysms in mice. Surgery 2005, 137, 457–462. [PubMed: 15800495]
25. Razavian M; Bordenave T; Georgiadis D; Beau F; Zhang J; Golestani R; Toczek J; Jung J-J; Ye Y; Kim H-Y; Han J; Dive V; Devel L; Sadeghi MM Optical imaging of MMP-12 active form in inflammation and aneurysm. Scientific reports 2016, 6, 38345–38345. [PubMed: 27917892]
26. Wang Y; Ait-Oufella H; Herbin O; Bonnin P; Ramkhelawon B; Taleb S; Huang J; Offenstadt G; Combadiere C; Renia L; Johnson JL; Tharaux PL; Tedgui A; Mallat Z TGF-beta activity protects against inflammatory aortic aneurysm progression and complications in angiotensin II-infused mice. J Clin Invest 2010, 120, 422–432. [PubMed: 20101093]
27. Johnson JL; Devel L; Czarny B; George SJ; Jackson CL; Rogakos V; Beau F; Yiotakis A; Newby AC; Dive V A selective matrix metalloproteinase-12 inhibitor retards atherosclerotic plaque development in apolipoprotein E-knockout mice. Arterioscler Thromb Vasc Biol 2011, 31, 528–535. [PubMed: 21212406]

28. Toczek J; Bordenave T; Gona K; Kim H-Y; Beau F; Georgiadis D; Correia I; Ye Y; Razavian M; Jung J-J; Lequin O; Dive V; Sadeghi MM; Devel L Novel matrix metalloproteinase 12 selective radiotracers for vascular molecular imaging. Journal of Medicinal Chemistry 2019, 62, 9743–9752. [PubMed: 31603669]
29. Borkakoti N Matrix metalloprotease inhibitors: design from structure. Biochemical Society Transactions 2004, 32, 17–20. [PubMed: 14748704]
30. Dorman G; Cseh S; Hajdu I; Barna L; Konya D; Kupai K; Kovacs L; Ferdinandy P Matrix metalloproteinase inhibitors: a critical appraisal of design principles and proposed therapeutic utility. Drugs 2010, 70, 949–964. [PubMed: 20481653]
31. Freskos JN; Asmelash B; Gaston KR; Karwa A; Marzan TA; Nickols MA; Rogers TE; Schoenstein T; Sympson CJ; Vu B Design and synthesis of MMP inhibitors with appended fluorescent tags for imaging and visualization of matrix metalloproteinase enzymes. Bioorg Med Chem Lett 2013, 23, 5566–5570. [PubMed: 23999043]
32. Serra P; Bruczko M; Zapico JM; Puckowska A; Garcia MA; Martin-Santamaria S; Ramos A; Pascual-Teresa B d. MMP-2 selectivity in hydroxamate-type inhibitors. Current Medicinal Chemistry 2012, 19, 1036–1064. [PubMed: 22257051]
33. Ye Y; Toczek J; Gona K; Kim HY; Han J; Razavian M; Golestani R; Zhang J; Wu TL; Ghosh M; Jung JJ; Sadeghi MM Novel arginine-containing macrocyclic MMP inhibitors: Synthesis, (99m)Tc-labeling, and evaluation. Sci Rep 2018, 8, 11647. [PubMed: 30076321]
34. Devel L; Czarny B; Beau F; Georgiadis D; Stura E; Dive V Third generation of matrix metalloprotease inhibitors: Gain in selectivity by targeting the depth of the S1' cavity. Biochimie 2010, 92, 1501–1508. [PubMed: 20696203]
35. Czarny B; Stura EA; Devel L; Vera L; Cassar-Lajeunesse E; Beau F; Calderone V; Fragai M; Luchinat C; Dive V Molecular determinants of a selective matrix metalloprotease-12 inhibitor: insights from crystallography and thermodynamic studies. Journal of medicinal chemistry 2013, 56, 1149–1159. [PubMed: 23343195]
36. Rouanet-Mehouas C; Czarny B; Beau F; Cassar-Lajeunesse E; Stura EA; Dive V; Devel L Zinc-metalloproteinase inhibitors: Evaluation of the complex role played by the zinc-binding group on potency and selectivity. Journal of medicinal chemistry 2017, 60, 403–414. [PubMed: 27996256]
37. Razavian M; Zhang J; Nie L; Tavakoli S; Razavian N; Dobrucki LW; Sinusas AJ; Edwards DS; Azure M; Sadeghi MM Molecular imaging of matrix metalloproteinase activation to predict murine aneurysm expansion in vivo. J Nucl Med 2010, 51, 1107–1115. [PubMed: 20554725]
38. Liu S; Edwards DS; Harris AR; Ziegler MC; Poirier MJ; Ewels BA; Diluzio WR; Hui P Towards developing a non-SnCl2 formulation for RP444, a new radiopharmaceutical for thrombus imaging. J Pharm Sci 2001, 90, 114–123. [PubMed: 11169528]
39. Curci JA; Liao S; Huffman MD; Shapiro SD; Thompson RW Expression and localization of macrophage elastase (matrix metalloproteinase-12) in abdominal aortic aneurysms. J Clin Invest 1998, 102, 1900–1910. [PubMed: 9835614]
40. Razavian M; Bordenave T; Georgiadis D; Beau F; Zhang J; Golestani R; Toczek J; Jung JJ; Ye Y; Kim HY; Han J; Dive V; Devel L; Sadeghi MM Optical imaging of MMP-12 active form in inflammation and aneurysm. Scientific reports 2016, 6, 38345. [PubMed: 27917892]
41. Daugherty A; Manning MW; Cassis LA Angiotensin II promotes atherosclerotic lesions and aneurysms in apolipoprotein E-deficient mice. J Clin Invest 2000, 105, 1605–1612. [PubMed: 10841519]
42. MMP12, lung function, and COPD in high-risk populations. New England Journal of Medicine 2010, 362, 1241–1242.
43. Butsch V; Borgel F; Galla F; Schwegmann K; Hermann S; Schafers M; Riemann B; Wunsch B; Wagner S Design, (radio)synthesis, and in vitro and in vivo evaluation of highly selective and potent matrix metalloproteinase 12 (MMP-12) inhibitors as radiotracers for positron emission tomography. J Med Chem 2018, 61, 4115–4134. [PubMed: 29660282]
44. Hagimori M; Temma T; Kudo S; Sano K; Kondo N; Mukai T Synthesis of radioiodinated probes targeted toward matrix metalloproteinase-12. Bioorganic & Medicinal Chemistry Letters 2018, 28, 193–195. [PubMed: 29191557]

45. Kondo N; Temma T; Aita K; Shimochi S; Koshino K; Senda M; Iida H Development of matrix metalloproteinase-targeted probes for lung inflammation detection with positron emission tomography. Scientific Reports 2018, 8, 1347. [PubMed: 29358724]
46. Su H; Spinale FG; Dobrucki LW; Song J; Hua J; Sweterlitsch S; Dione DP; Cavaliere P; Chow C; Bourke BN; Hu XY; Azure M; Yalamanchili P; Liu R; Cheesman EH; Robinson S; Edwards DS; Sinusas AJ Noninvasive targeted imaging of matrix metalloproteinase activation in a murine model of postinfarction remodeling. Circulation 2005, 112, 3157–3167. [PubMed: 16275862]
47. Reichelt A; Gaul C; Frey RR; Kennedy A; Martin SF Design, synthesis, and evaluation of matrix metalloprotease inhibitors bearing cyclopropane-derived peptidomimetics as P1' and P2' replacements. J Org Chem 2002, 67, 4062–4075. [PubMed: 12054939]
48. Wojtowicz-Praga S; Torri J; Johnson M; Steen V; Marshall J; Ness E; Dickson R; Sale M; Rasmussen HS; Chiodo TA; Hawkins MJ Phase I trial of Marimastat, a novel matrix metalloproteinase inhibitor, administered orally to patients with advanced lung cancer. J Clin Oncol 1998, 16, 2150–2156. [PubMed: 9626215]
49. Matter H; Schudok M Recent advances in the design of matrix metalloprotease inhibitors. Curr Opin Drug Discov Devel 2004, 7, 513–535.
50. Chen JM; Nelson FC; Levin JI; Mobilio D; Moy FJ; Nilakantan R; Zask; Arie; Powers R Structure-based design of a novel, potent, and selective inhibitor for MMP-13 utilizing NMR spectroscopy and computer-aided molecular design, J. Am. Chem. Soc 2000, 122, 9648–9654.
51. Engel CK; Pirard B; Schimanski S; Kirsch R; Habermann J; Klingler O; Schlotte V; Weithmann KU; Wendt KU Structural basis for the highly selective inhibition of MMP-13. Chemistry & Biology 2005, 12, 181–189. [PubMed: 15734645]
52. Ikejiri M; Bernardo MM; Meroueh SO; Brown S; Chang M; Fridman R; Mobashery S Design, synthesis, and evaluation of a mechanism-based inhibitor for gelatinase A. The Journal of Organic Chemistry 2005, 70, 5709–5712. [PubMed: 15989356]
53. Devel L; Rogakos V; David A; Makaritis A; Beau F; Cuniasse P; Yiotakis A; Dive V Development of selective inhibitors and substrate of matrix metalloproteinase-12. J Biol Chem 2006, 281, 11152–11160. [PubMed: 16481329]
54. Bencsik P; Kupai K; Görbe A; Kenyeres É; Varga ZV; Pálóczi J; Gáspár R; Kovács L; Weber L; Takács F; Hajdú I; Fabó G; Cseh S; Barna L; Csont T; Csonka C; Dormán G; Ferdinandy P Development of matrix metalloproteinase-2 inhibitors for cardioprotection. Frontiers in Pharmacology 2018, 9.
55. Toczek J; Bordenave T; Gona K; Kim HY; Beau F; Georgiadis D; Correia I; Ye Y; Razavian M; Jung JJ; Lequin O; Dive V; Sadeghi MM; Devel L Novel matrix metalloproteinase 12 selective radiotracers for vascular molecular imaging. J Med Chem 2019, 62, 9743–9752. [PubMed: 31603669]
56. Bordenave T; Helle M; Beau F; Georgiadis D; Tepshi L; Bernes M; Ye Y; Levenez L; Poquet E; Nozach H; Razavian M; Toczek J; Stura EA; Dive V; Sadeghi MM; Devel L Synthesis and in vitro and in vivo evaluation of MMP-12 selective optical probes. Bioconjug Chem 2016, 27, 2407–2417. [PubMed: 27564088]
57. Horovitz A; Levitzki A An accurate method for determination of receptor-ligand and enzyme-inhibitor dissociation constants from displacement curves. Proceedings of the National Academy of Sciences 1987, 84, 6654.

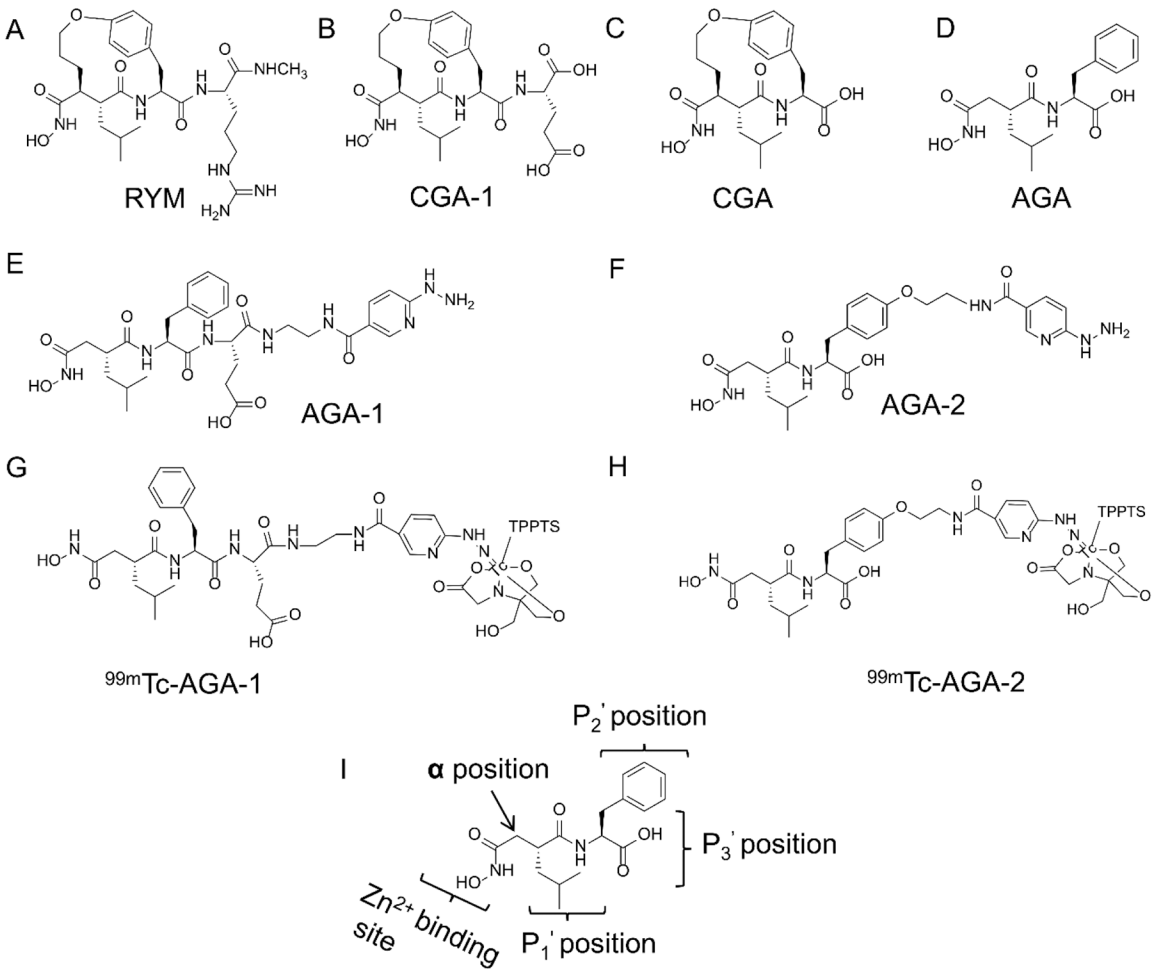

Figure 1.

Chemical structures of the panMMP inhibitor RYM (A), and novel cyclic MMP-12 inhibitors CGA-1 (B) and CGA (C), as well as the novel acyclic MMP-12 inhibitor AGA (D), radiolabeling precursors AGA-1 (E) and AGA-2 (F), and their corresponding ^{99m}Tc-labelled SPECT imaging agents ^{99m}Tc-AGA-1 (G) and ^{99m}Tc-AGA-2 (H). The key structural components of AGA and the structure activity relationship used to develop novel MMP-12-selective inhibitors and SPECT imaging agents are shown in panel (I).

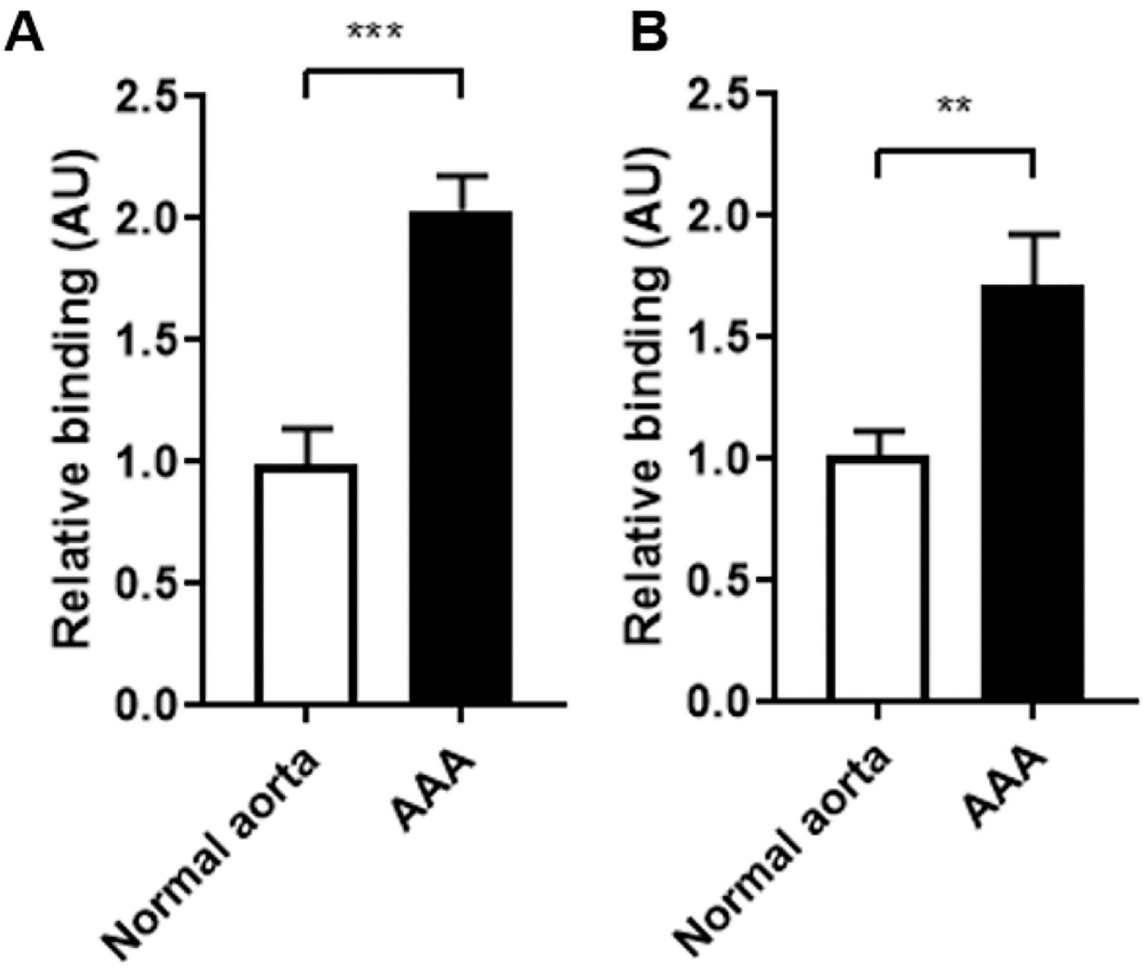

Figure 2.

Ex vivo binding of ^{99m}Tc-AGA-1 (A), ^{99m}Tc-AGA-2 (B) to human normal aorta and AAA tissue. n = 3 in each group, $^{**}P < 0.01$, $^{***}P < 0.001$. AU: arbitrary units.

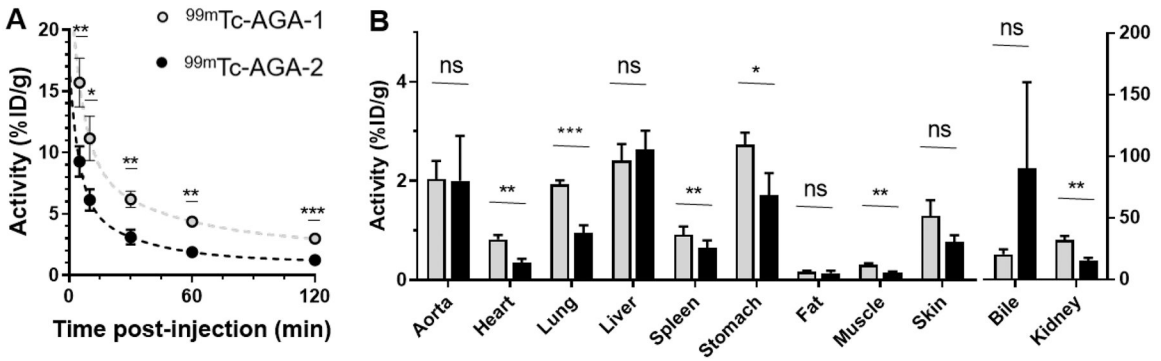

Figure 3.

MMP-12 tracer biodistribution and clearance. Blood kinetics (A) and biodistribution (B) at 2 h after ^{99m}Tc-AGA-1 and ^{99m}Tc-AGA-2 administration in C57BL/6J mice. ID = injected dose. n = 3 in each group, $*P < 0.05$, $**P < 0.01$, $***P < 0.001$ (t-test).

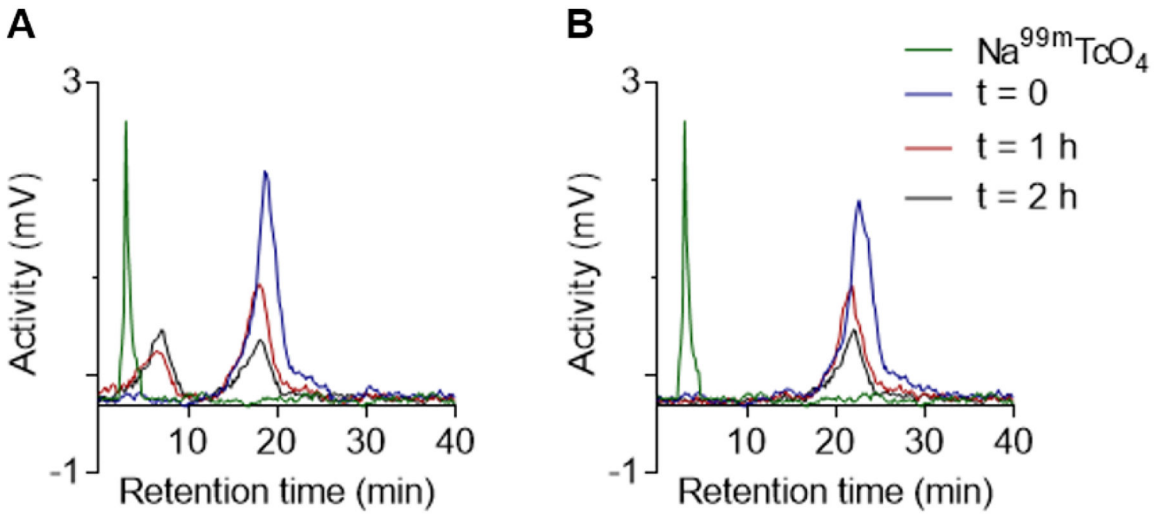

Figure 4.

MMP-12 tracer stability in mouse blood. Representative radiochromatograms of $Na^{99m}TcO_4$ (green lines), and ^{99m}Tc-AGA-1 (A) and ^{99m}Tc-AGA-2 (B) immediately after radiolabeling (blue lines), after 1 h (red lines) and after 2 h (grey lines).

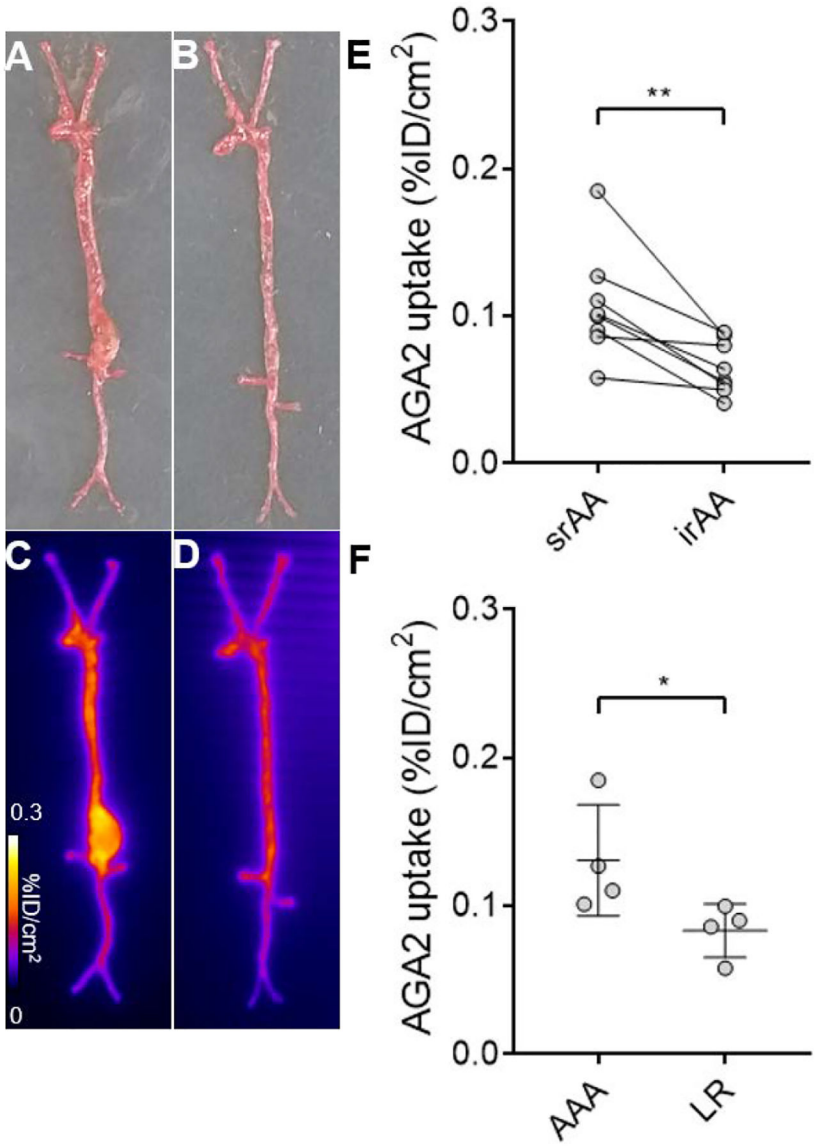

Figure 5.

MMP-12 imaging in AAA. Examples of ex vivo photographs (A, B), and corresponding autoradiographs after 2 h post injection of ^{99m}Tc-AGA-2 (C, D) of aortae from Ang II induced *Apoe*$^{-/-}$ mice with abdominal aortic aneurysm (A, C), and low remodeled aorta (B, D). E) Quantification of the ^{99m}Tc-AGA-2 signal in suprarenal abdominal aorta (srAA) and infrarenal abdominal aorta (irAA) of Ang II infused mice, n = 8, $^{**}P < 0.01$, paired t-test. (F) Quantification of the ^{99m}Tc-AGA-2 signal in animals with AAA and low remodeled (LR) aorta, n= 4 in each group, $^{*}P < 0.05$, Mann-Whitney U test. ID: injected dose.

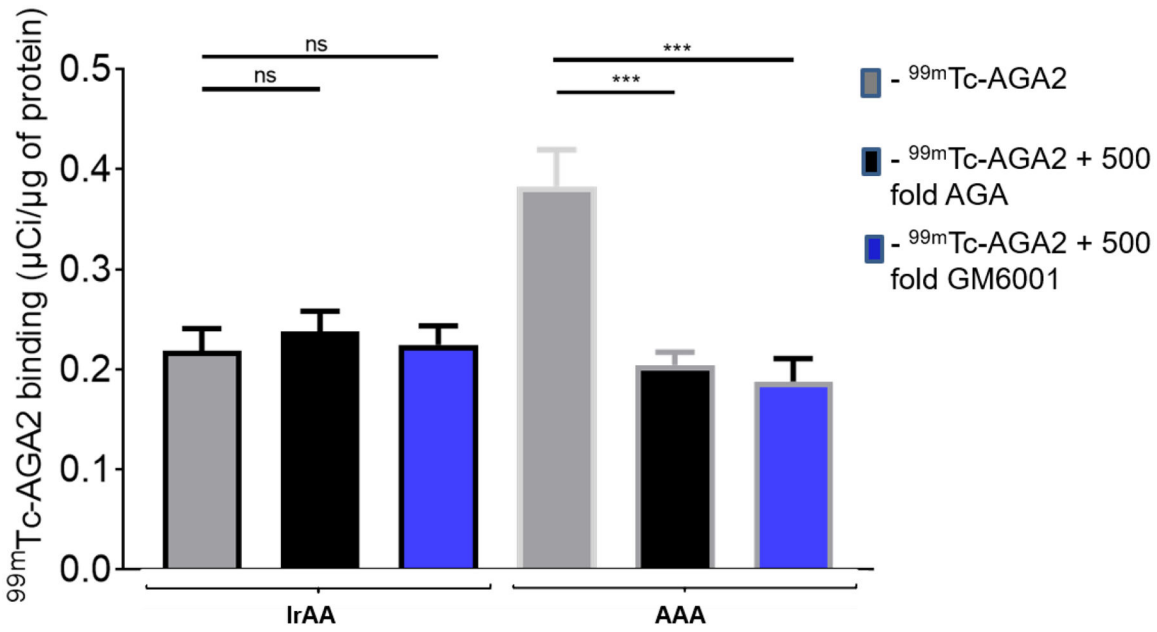

Figure 6.

^{99m}Tc-AGA2 binding specificity. Ex vivo binding of ^{99m}Tc-AGA2 to mouse infrarenal aorta (irAA) and AAA tissue without (gray columns) and with co-incubation with 500 molar fold excess MMP-12-specific inhibitor (AGA, yellow columns), or panMMP inhibitor (GM6001, green columns), n = 3 for each group. ns: not significant, ***$P < 0.001$, one-way ANOVA.

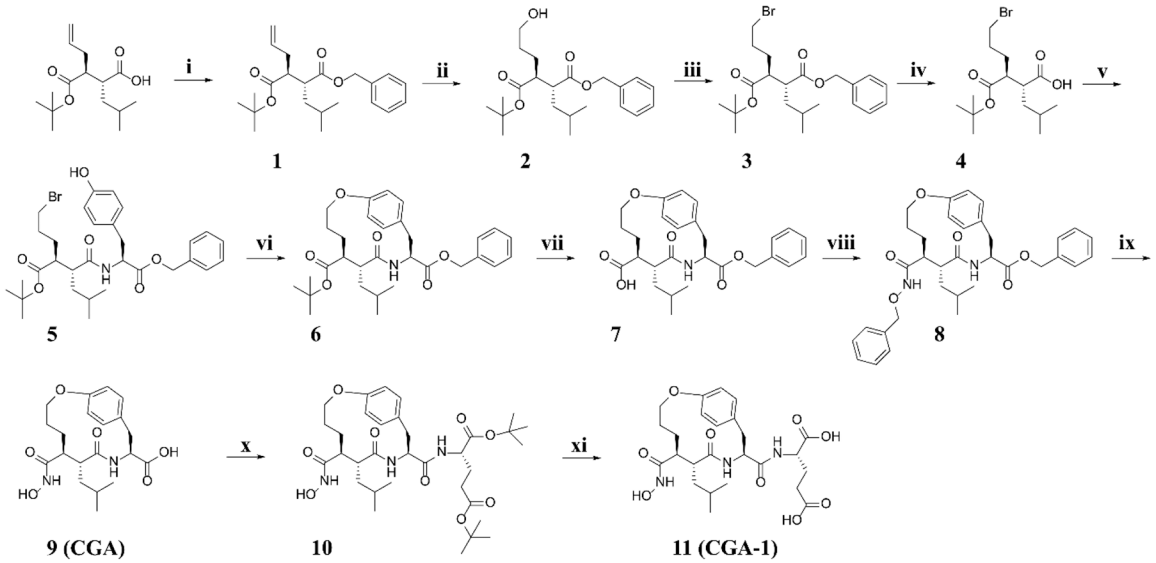

Scheme 1.

Synthetic scheme for preparation of CGA & CGA-1. Reagents & Conditions: **i**. BnBr/DBU/Toluene/RT/2 h & 60 °C/1 h/Yield 71%; **ii**. a) 9-BBN/THF; b) H_2O_2/H_2O/RT/12 h/Yield 70%; **iii**. CBr_4/Ph_3P/DCM/RT/Yield 63%; **iv**. Pd/C(10%)/H_2/CH_3OH/RT/30 min/Yield 85%; **v**. H-Tyr-OBz/EDCI/HOBT/DMF/RT/12 h/Yield 74%; **vi**. Cs_2CO_3/Acetonitrile/RT/6 h/Yield 55%; **vii**. TFA/DCM/RT/2 h/Yield 100%; **viii**. Bz-ONH2/HOAT/HATU/DIPEA/DMF/RT/18 h/ Yield 62%; **ix**. Pd/C(10%)/H_2/CH_3OH/RT/2 h/Yield 58%; **x**. Glu-di-t-butyl ester/EDCI/HOBT/DMF/RT/18 h/Yield 25%; **xi**. TFA/DCM/RT/2 h/Yield 8%.

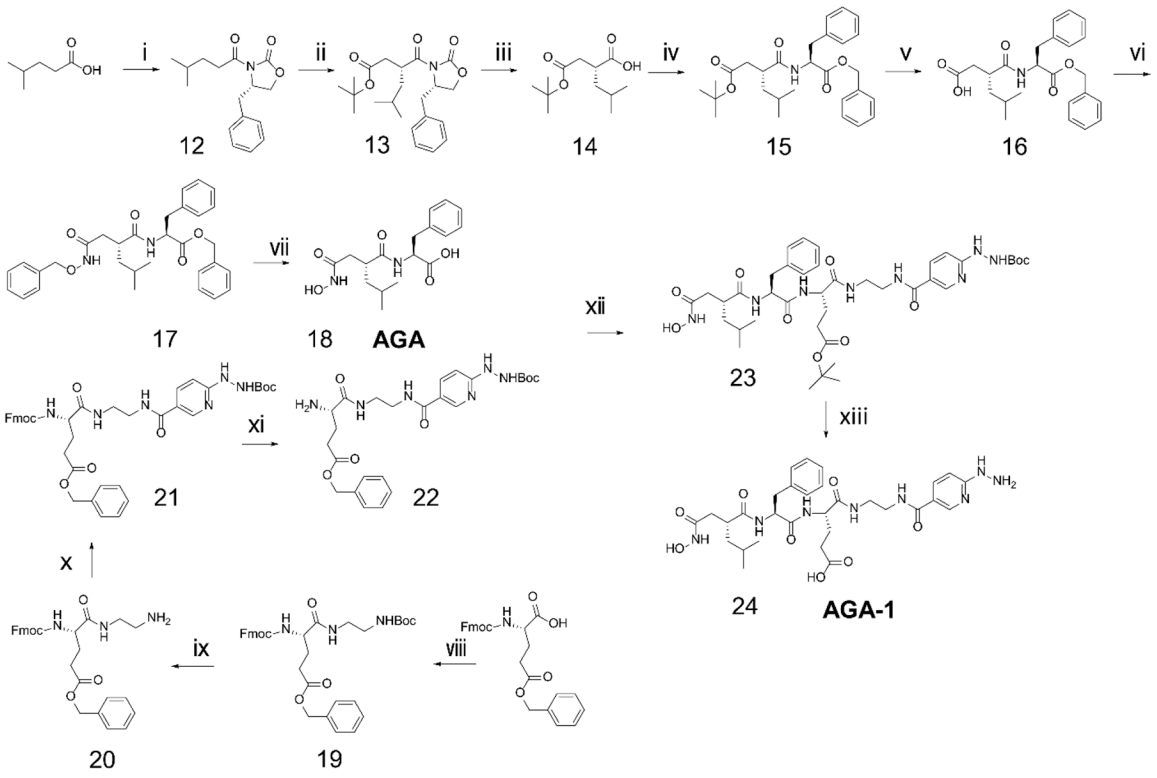

Scheme 2.

Synthetic scheme for preparation of AGA & AGA-1. Reagents & Conditions: **i**. PivCl/ LiCl/0 °C/2 h/S-Benzyl oxazolidinone/THF/−78 °C to RT/12 h/Yield 55%; **ii**. NaHMDS(1.9M)/Br-CH_2CO_2-t-Bu/THF/−78 °C to RT/12 h/Yield 62%; **iii**. LiOH/ H_2O_2/THF/0 °C to RT/2 h/Yield 75%; **iv**. L-Phenylalanine benzyl ester/EDCI/ HOBT/DMF/RT/18 h/Yield 72%; **v**. TFA/DCM/RT/2 h/Yield 100%; **vi**. Bz-ONH2/BOP/ DIEA/DMF/RT/18 h/Yield 80%; **vii**. Pd/C(10%)/H_2/CH_3OH/RT/2 h/Yield 62%; **viii**. Boc-NH-CH2CH2-NH2/ Fmoc-Glu(O-Bz)-OH/EDCI/HOBT/DMF/0 °C to RT/2.5 h/Yield 72%; **ix**. TFA/DCM/RT/30 min/Yield 72%; **x**. N-Boc-HYNIC acid/ EDCI/HOBT/ DIEA/DMF/RT/18 h/Yield 55%; **xi**. Piperdine/DCM/RT/30 min/Yield 65%; **xii**. 2.7/2.11/ EDCI/HOBT/DIPEA/DMF/RT/18 h/Yield 45%; **xiii**. a) TFA/DCM/RT/2 h; b) Pd/ C(10%)/H_2/CH_3OH/RT/2 h/Yield 14%.

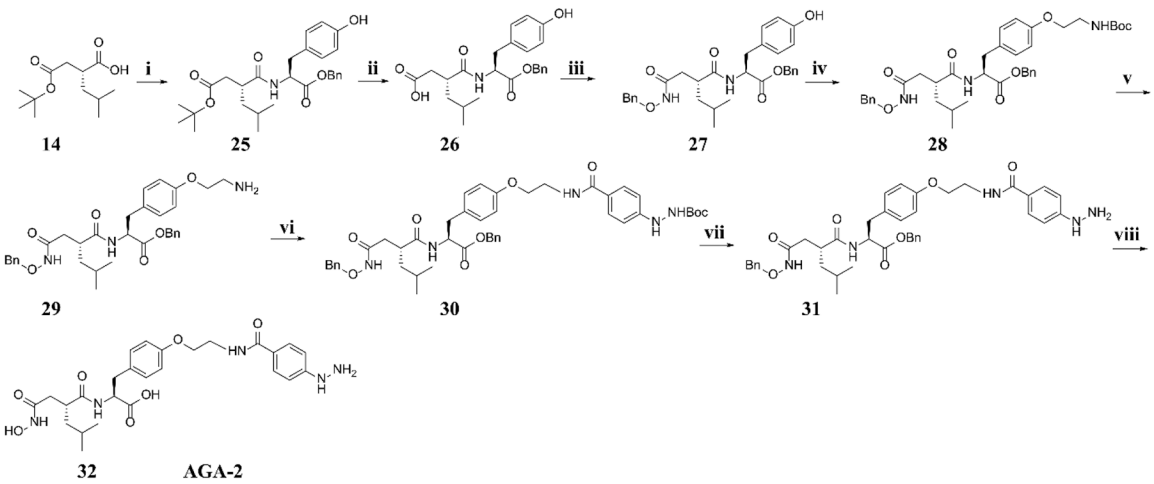

Scheme 3.

Synthetic scheme for preparation of AGA-2. Reagents & Conditions: **i**. H-Tyr-OBz/EDCI/HOBT/DMF/RT/18 h/Yield 65%; **ii**. TFA/DCM/RT/2 h/Yield 100%; **iii**. Bz-ONH2/HBTU/DIEA/DMF/RT/18 h/Yield 66%; **iv**. 2-(BOC-amino)ethyl bromide/Cs_2CO_3/Acetonitrile/60 °C/4 h/Yield 58%; **v**. TFA/DCM/RT/2 h/Yield 100%; **vi**. N-Boc-HYNIC acid/ HOAT/HATU/DIEA/DMF/RT/18 h/Yield 53%; **vii**. TFA/DCM/RT/Yield 100%; **viii**. Pd/C(10%)/H_2/CH_3OH/RT/ 2 h/Yield 9%.

Table 1.

Inhibition constants (K_i) of AGA, CGA, CGA-1 and RYM. K_i values represent the mean ± SD of three experiments.

Ki (nM)	rhMMP-2	rhMMP-7	rhMMP-9	rhMMP-12	rhMMP-13
CGA	300 ± 81	39 ± 2.0	1101 ± 289	1.1 ± 0.6	31 ± 12
CGA-1	396 ± 28	14.6 ± 0.1	2107 ± 454	1.2 ± 0.1	89 ± 18
RYM	5.8 ± 0.4	17.2 ± 0.1	20.4 ± 2.0	1.0 ± 0.5	15.3 ± 5.4
AGA	164 ± 43	323 ± 129	125 ± 14	11.8 ± 1	81 ± 33
AGA-1	222 ± 17	615 ± 53	1305 ± 204	7.5 ± 1.4	78 ± 5
AGA-2	> 5 μM	> 5 μM	155 ± 14	8.9 ± 0.2	> 5 μM